IEEE Open Journal of
Industry Applications

Received 27 September 2019; revised 13 November 2019; accepted 26 November 2019. Date of publication 3 December 2019; date of current version 2 January 2020. The review of this article was arranged by Associate Editor S. Odhano.

Digital Object Identifier 10.1109/OJIA.2019.2956987

Shaft Failure Analysis in Soft-Starter Fed Electrical Submersible Pump Systems

SHEIKH F. RABBI [1], JALAL TAHERI KAHNAMOUEI[2], XIAODONG LIANG [3] (Senior Member, IEEE), AND JIANMING YANG[2]

[1]Department of Electrical and Computer Engineering, Memorial University of Newfoundland, St. John's, NL A1B 3X5, Canada
[2]Department of Mechanical Engineering, Memorial University of Newfoundland, St. John's, NL A1B 3X5, Canada
[3]Department of Electrical and Computer Engineering, University of Saskatchewan, Saskatoon, SK S7N 5A9, Canada

CORRESPONDING AUTHOR: XIAODONG LIANG (e-mail: xil659@mail.usask.ca)

This work was supported in part by the Natural Sciences and Engineering Research Council of Canada's Collaborative Research and Development Grant: NSERC CRDPJ 517822 - 17.

ABSTRACT Electric submersible pumps (ESPs) are widely used for high volumetric oil and gas recovery from downhole wells. ESPs in oil fields can be equipped with multiple ac motors in tandem. To assist a motor start-up, a solid-state soft-starter can be deployed in such ESP wells. ESP shafts have a long axial length, and thus experience significant dynamic torsion when started from reduced voltage soft-starters. Premature shaft breakdowns had occurred in the field during the motor start-up for soft-starter fed ESPs. This paper investigates the shaft breakdown phenomenon in a 750-HP ESP system using a real-world case scenario. A lumped parameter electro-mechanical model for the ESP system is developed to observe its dynamics. The effects of static as well as fluctuating torsional stress on the interconnected pump shafts are analyzed to determine the root cause of the shaft breakdown. Criteria for successful start-up for soft-starter driven ESP systems are also presented to increase the equipment's operational life.

INDEX TERMS Electric submersible pump, induction motors, soft-starter, shaft dynamics, torsional vibration, fatigue analysis.

I. INTRODUCTION

AN ELECTRIC submersible pump (ESP) is an artificial lift technique commonly used for oil and gas recovery from downhole reservoirs. It consists of multi-stage rotating impeller blades driven by medium voltage electric submersible AC motors. The pump-motor assembly in an ESP system is placed inside a downhole well, located hundreds to several thousands of feet below the surface. The pump blades while spinning increases the pressure of the reservoir fluid and forces it to reach the surface. The rate of oil recovery depends on the pressure produced by the ESP and is adjustable by varying the speed of the motor. Thus, ESPs can achieve a wide rate of production ranging from 200 to over 20,000 barrels of fluids per day [1]. Since the inception of ESPs, three-phase squirrel-cage induction submersible motors have been the de-facto technology as the prime mover. On the surface, the power supply to the submersible motor can be either a switchboard or a variable frequency drive (VFD) through a lengthy downhole cable. An ESP motor start-up directly from a switchboard supply creates a large starting current, which can be 6 to 9 times of the motor rated current, and thus introduces severe mechanical stress in the system [2]–[6]. This may expose the ESP shafts and interconnections to overload conditions and result in ESP failures [7]–[9]. Extended exposure to a fluctuating mechanical stress can also introduce fatigue in the system.

Sustained fatigue with a high level of mechanical stress may break the shaft and connectors at a premature stage. Thus, soft-starters are deployed for submersible motors to reduce the stress on the electrical power supply and the mechanical transmission system [10]–[12]. Classical solid-state soft-starters are equipped with thyristors in series with the line that only regulates the applied voltage to the motor while keeping the supply frequency constant. In recent years, VFDs have been increasingly used in oil fields that can regulate both the frequency and voltage during start-up and normal operation of an ESP system [13]–[16]. Although VFDs are gaining popularity, solid-state soft-starters for switchboard supply

are still widely used for operating induction motors in ESP systems.

Starting an ESP system from a switchboard supply either directly on-line or through soft-starter creates severe torsional vibration in the electromechanical assembly [17]–[19]. The unique ESP shaft geometry (long length and small diameter) is primarily accountable for it. Severe torsional vibration may occur if the vibrational frequency of the shaft reaches its resonant value. Thus, it is necessary to develop a dynamic model of an ESP system to observe the electromechanical transients during its start-up. One way to accurately model the electromechanical dynamics of an ESP system is the multi-physics simulation using finite element analysis [20]. However, multi-physics simulation is resource exhaustive and computationally overburdened. Another way is the approximate lumped parameter approach [3], [4]. Few researchers have proposed lumped parameter models to combine electrical and mechanical dynamics of induction motor driven ESP systems to investigate the events associated with the start-up of an ESP system [4]. The start-up transient mechanical stress on the pump assembly for direct on-line starting condition is observed in [3]. The effects of different shaft diameters as well as shaft lengths on the starting torsional vibration in ESPs are also presented in [3]. In [21]–[24], the causes for torsional vibration induced failures in ESP systems are investigated using different case studies along with a general guideline to avoid these types of failures. A relative comparison between different types of starting methods for medium voltage induction motor drives are provided in [22]. Start-up dynamics of a soft-starter fed ESP system is investigated by few researchers using numerical simulations [4]–[7]. A root cause analysis for shaft failures in AC motor drives is presented in [21]. The effects of rotor inertia on the acceleration time are also analyzed in [10]. Although the existing literature shows the existence of severe torsional oscillations during starting of large induction motor drives, it does not analyze the effects of the induced high dynamic torsional stress on the mechanical integrity of the system. The relatively short run-life of ESPs which can be less than 30 days are often due to failures in their shaft/coupler assembly. Starting failures including shaft/coupler breakdowns due to severe fatigue are relatively common phenomena for soft-starter fed ESPs operating in downhole oil wells. The existing literature does not provide an in-depth analysis for the shaft breakdown failures involved with fixed frequency reduced voltage soft-starter fed ESP drives. The total cost to replace or repair an ESP unit is very high and failures in ESPs create long downtime in the oil field. Thus, a comprehensive study using torsional dynamics of a real-world ESP system to determine the root cause for failures during start-up and identify preventive measures to avoid premature ESP failures to extend their operational run life is urgently needed by the oil and gas industries.

This paper presents a systematic root cause analysis for shaft breakdown phenomena in a soft-starter driven 750-HP ESP system during its practical oil field application in a shallow well. The main contribution of this paper includes: 1) The performance of the soft-starter on reducing electrical as well mechanical stress for the ESP drive system is analyzed; 2) A torsional vibration analysis is carried out to observe the influence of torque oscillations on the mechanical shaft dynamics in the ESP system; 3) An analysis of fatigue is carried out to demonstrate how consecutive start-up failures introduces extreme fatigue in the system and create shaft breakdowns due to cyclic torsional stress; 4) A safe start-up procedure for soft-starting the ESP motor is recommended to increase its run life.

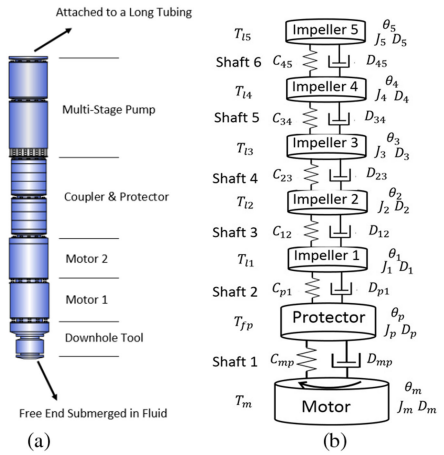

FIGURE 1. (a) A typical configuration of an ESP system, (b) a lumped parameter model of an ESP system.

This paper is organized as follows: Section II provides a simplified modeling of the ESP system dynamics. Section III explains the reduced voltage starting of an ESP system using a real world 750-HP soft-starter fed ESP well through different star-up conditions. The torsional dynamic analysis of the ESP system for various operating conditions is carried out in Section IV. Section V analyzes the fatigue in the ESP shaft to determine the root cause of the broken shaft. Conclusions are drawn in Section VI.

II. MODELING OF ESP DYNAMICS

Fig. 1(a) displays a typical configuration of an electric submersible pump. The downhole motor unit is placed at the bottom of the ESP string. The multi-stage pump unit is attached to the motor through a coupler/protector that prohibits any fluids from entering inside of the motor. For high power ESPs, multiple electric motors are connected in tandem to provide the adequate torque for achieving the required pump head and flow rate. Each motor in an ESP has a long narrow stator and a plurality of rotors connected in series. The motor shaft normally has a higher diameter than the pump shafts. The coupler accounts for the changes in the shaft diameter.

Fig. 1(b) illustrates a lumped parameter electro-mechanical model of an ESP system with five pump stages to represent the drive system dynamics. The tandem series connection of induction motor windings is displayed in Fig. 2. The motor windings are connected in series to form a 3-phase star topology. The mechanical dynamics of the ESP system are

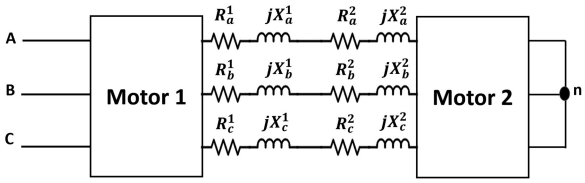

FIGURE 2. Tandem series connection of induction motor windings.

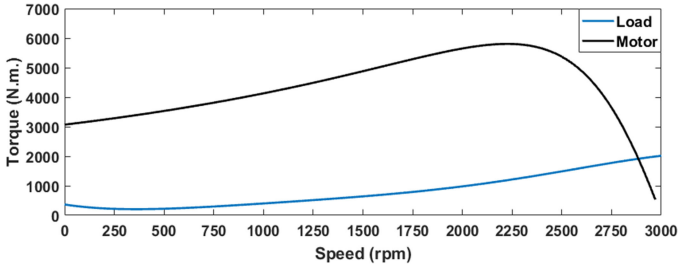

FIGURE 3. Average motor and load torque characteristics in an ESP.

modelled as a torsional mass spring damper system similar to [3]. The shafts are assumed flexible and their stiffness and damping are calculated from the physical dimensions (length and diameter). The equations for modeling ESP dynamics are provided as follows:

For the Motor:

$$J_m \frac{d^2\theta_m}{dt^2} + D_m \frac{d\theta_m}{dt} + D_{mp}\left(\frac{d\theta_m}{dt} - \frac{d\theta_1}{dt}\right) + C_{mp}\left(\theta_m - \theta_1\right) = T_m \tag{1}$$

For the Protector:

$$J_p \frac{d^2\theta_p}{dt^2} + D_{mp}\left(\frac{d\theta_p}{dt} - \frac{d\theta_m}{dt}\right) + C_{mp}\left(\theta_p - \theta_m\right) + D_{p1}\left(\frac{d\theta_p}{dt} - \frac{d\theta_1}{dt}\right) + C_{p1}\left(\theta_p - \theta_1\right) = -T_{fp} \tag{2}$$

For Impeller 1 and 2:

$$J_1 \frac{d^2\theta_1}{dt^2} + D_1 \frac{d\theta_1}{dt} + D_{p1}\left(\frac{d\theta_1}{dt} - \frac{d\theta_p}{dt}\right) + C_{p1}\left(\theta_1 - \theta_p\right) + D_{12}\left(\frac{d\theta_1}{dt} - \frac{d\theta_2}{dt}\right) + C_{12}\left(\theta_1 - \theta_2\right) = -T_{l1} \tag{3}$$

The dynamics for impellers 2-4 can be described similarly using (3). The dynamics for impeller 5 is given below**:**

$$J_5 \frac{d^2\theta_5}{dt^2} + D_5 \frac{d\theta_5}{dt} + D_{45}\left(\frac{d\theta_5}{dt} - \frac{d\theta_4}{dt}\right) + C_{45}\left(\theta_5 - \theta_4\right) = -T_{l5} \tag{4}$$

where J_m and J_p are the inertia of the motor and the protector, respectively; $J_1 \ldots J_5$ are the inertia of impellers 1 …5, respectively; D_m, D_p and D_{mp} are the viscous damping coefficient of the motor, its protector and the interconnecting shaft between them, respectively; T_{fp} is the friction torque in the protector; $T_{l1} \ldots T_{l5}$ are the load torque of impellers 1 …5, respectively; C_{mp} and $C_{p1}$are the compliance (inverse of stiffness) of the shaft between motor and protector, and protector and impeller 1, respectively; C_{12}, C_{23}, C_{34} and C_{45} are the compliance of the shafts between the impellers 1 …5, respectively; D_{12}, D_{23}, D_{34} and D_{45} are the viscous damping coefficient of the shafts between the impellers 1 …5, respectively; $D_1 \ldots D_5$ are the viscous damping coefficient of the impellers 1 …5, respectively; θ_m is the angular position of the motor; and θ_1 … θ_5 are the angular positions of the impellers 1 …5, respectively.

The electrical equivalent circuit parameters for series connected tandem induction motors are determined based on the data from individual motor test results. The equivalent stator and rotor resistances, and leakage inductances are calculated by

$$R_1^t = \sum_{i=1}^{n} R_1^i;\ L_1^t = \sum_{i=1}^{n} L_1^i;\ R_2^t = \sum_{i=1}^{n} R_2^i; L_2^t = \sum_{i=1}^{n} L_2^i \tag{5}$$

where, R_1^i and L_1^i are the stator resistances and leakage inductace of i^{th} motor, respectively, R_2^i and L_2^i are the rotor resistances and leakage inductances, respectively, and n is the number of motors connected in series. The equivalent magnetizing inductance L_m^t of the tandem motors can be obtained using the following expression [25],

$$L_m^t = \sum_{i=1}^{n} \frac{3\pi}{8} N_{se,i}^2 \frac{\mu_0 l_i r}{g_e} \tag{6}$$

where $N_{se,i}$ is the effective number of series turns per phase of i^{th} motor, μ_0 is the magnetic permeability of air, l_i is the total length of the motors connected in series, r is the mean radius of the air-gap and g_e is the effective length of the air-gap. For identical motors connected in tandem, the equivalent magnetizing inductance can be calculated using (6),

$$L_m^t = iL_m \tag{7}$$

where i is the number of motors connected in tandem and L_m is the magnetizing inductance of each motor. The average motor torque T_m can be expressed as follows [25]:

$$T_m = \frac{3}{\omega_s} \frac{{V_{th}}^2 \left(\frac{R_2^t}{s}\right)}{\left(R_{th} + \frac{R_2^t}{s}\right)^2 + \left(X_{th} + X_2^t\right)^2} \tag{8}$$

where ω_s and s are the synchronous angular speed and the slip of the rotor, respectively, V_{th}, R_{th} and X_{th} are Thevenin equivalent voltage, resistance and reactance, respectively. X_2^t is the equivalent rotor reactance. The Thevenin equivalent circuit parameters are calculated using R_1^t, L_1^t and L_m^t.

The torque characteristics of the pump load and the motor in an ESP system is illustrated in Fig. 3. The expression of the load torque contains a static part, T_{l0} which depends on the inertia and the static friction, and a dynamic part T_{ld} that is related to the speed of the pump, and it can be expressed as

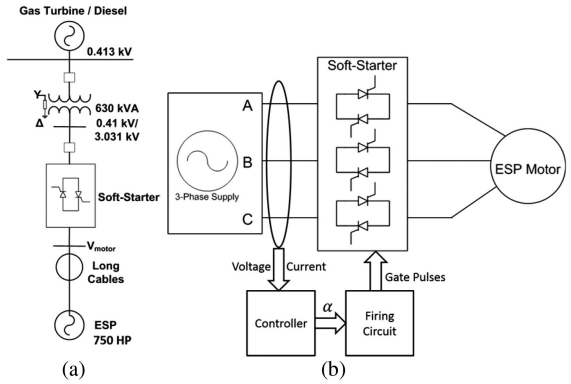

FIGURE 4. **(a) A single line diagram of an ESP system, and (b) a soft-starter.**

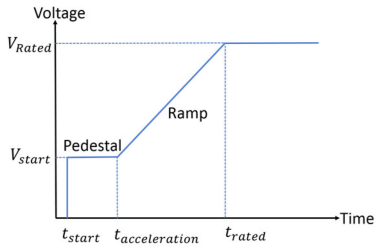

FIGURE 5. **Output settings for a solid state soft-starter.**

follows,

$$T_l = T_{l0} + T_{ld};\ T_{ld} = an^5 + bn^4 + cn^3 + dn^2 + en \quad (9)$$

where a, b, c, d and e are the load torque coefficients and n is the rotational speed (p.u.) of the pump. The static load torque that the motor must overcome to accelerate an ESP can be anywhere between 10%–25% of the motor rated torque. Thus, the starting motor torque requirement can be significantly high during soft-starting an ESP system to maintai a sufficient rotor acceleration to pass the critical speed swiftly for avoiding severe torsional oscillations.

III. SOFT-STARTING OF ESP SYSTEMS

In this paper, we use a real world 750-HP soft-starter fed ESP well to conduct the study. This well had experienced broken motor shafts during several attempts of the motor start-up. Fig. 4(a) illustrates the electrical single line diagram of the ESP system. The transformer is rated at 630 kVA, its primary rated voltage is 410 V, and its secondary tap setting is 3031 V. The total length of the cable is 184 meters cables including a 154 m downhole cable and a 30 m motor lead extension cable. The motor unit consists of two 3-phase AC induction motors in tandem series configuration. The whole motor unit is rated at 750 HP and 3100 V@50 Hz. Detailed specifications of the ESP system are provided in Table I in the Appendix. Fig. 4(b) presents the internal system configuration of a solid state soft-starter. A set of back-to-back thyristors are placed in series with the line to control the phase angle of the supply voltage to regulate the starting current for the motor. Fig. 5

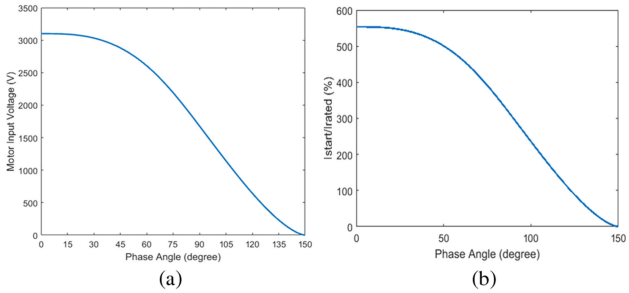

FIGURE 6. **Performance of the soft-starter fed ESP motor: (a) motor input voltage vs. phase angle and (b) starting current vs. phase angle.**

illustrates a standard output setting for an open loop solid state soft-starter. The starting voltage V_{start} of the soft-starter can be anywhere between 25%–50%, depending on the load torque and inertia. The acceleration time is related to the system inertia. A quick acceleration to rated applied voltage will start the motor quickly but will result in a high starting current and torque; while a slow acceleration may result in resonance causing mechanical failures such as shaft breakdowns.

The output phase voltage controlled by the soft-starter can be expressed as follows [26]:

$$V_o = \sqrt{6}V_s\sqrt{\left[\frac{1}{\pi}\left(\frac{\pi}{6} - \frac{\alpha}{4} + \frac{\sin 2\alpha}{8}\right)\right]};\ \text{for } 0 \le \alpha < 60^0 \quad (10)$$

$$V_o = \sqrt{6}V_s\sqrt{\left[\frac{1}{\pi}\left(\frac{\pi}{12} + \frac{3\sin 2\alpha}{16} + \frac{\sqrt{3}\cos 2\alpha}{16}\right)\right]};\ \text{for } 60^0 \le \alpha < 90^0 \quad (11)$$

$$V_o = \sqrt{6}V_s\sqrt{\left[\frac{1}{\pi}\left(\frac{5\pi}{24} - \frac{\alpha}{4} + \frac{\sin 2\alpha}{16} + \frac{\sqrt{3}\cos 2\alpha}{16}\right)\right]};\ \text{for } 90^0 \le \alpha \le 150^0: \quad (12)$$

where V_s and V_0 are the input and output phase voltages for the soft-starter, respectively, and α is the trigger/phase angle.

The starting torque of an induction motor is proportional to the square of the applied input voltage as indicated in (8). The relationship between the phase angle and the input voltage to an ESP motor is depicted in Fig. 6(a). The starting current varies with the phase angle as shown in Fig. 6(b). For $\alpha = 0^0$, the motor experiences a full rated voltage across the line, resulting in a starting current over 500% of its rating. High starting current imposes severe electrical stress in the power system and create a significant voltage dip across the line. Thus, soft-starters are used to limit the starting current for an ESP system by applying a high phase angle during the start-up.

Figs. 7(a) and 7(b) displays the relationship of starting torque vs. phase angle or starting current of the motor. The starting torque does not increase linearly with the starting current as shown in Fig. 7(b). Thus, limited starting current

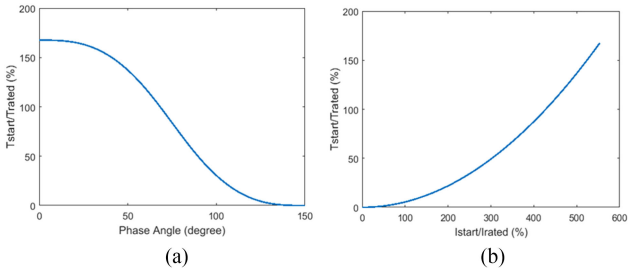

FIGURE 7. Performance of the soft-starter fed ESP motor: (a) starting torque vs. phase angle and (b) starting torque vs. starting current.

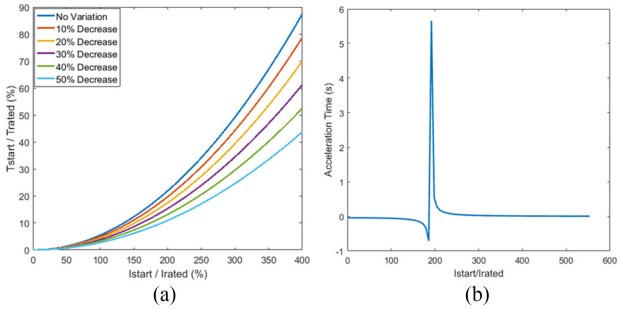

FIGURE 8. (a) Effects of rotor resistance variation on the motor starting torque; (b) acceleration time of the motor vs. starting current.

reduces the output torque for the motor significantly. For example, a 250% starting current only generates around 30% of the motor rated torque and requires the phase angle to be higher than 100^0 which decreases the power factor and induces higher harmonics in the system. Rotor resistance also varies due to skin effects and saturation phenomena which may exacerbates the starting of an ESP system by lowering the effective motor torque [27], [28]. The actual effective rotor resistance may be as much as 50% less than its calculated value from the locked rotor test. Fig. 8(a) illustrates the effect of rotor resistance variations on the motor output torque. Thus, selecting the appropriate starting phase angle for the motor is important.

The starting time to accelerate an ESP plays a critical role in its torsional dynamics. The acceleration time for an ESP drive can be calculated using the following equation [10],

$$t_a = \frac{\left(WK^2 + LWK^2\right)\ \Delta S}{308\ \Delta T} \tag{13}$$

Where, t_a is acceleration time, WK^2 is the inertia of the motor in lb-ft^2, LWK^2 is the inertia of the motor in lb-ft^2, ΔS is the change is speed during the time in rpm, and ΔT is the average acceleration torque in lb-ft. The average acceleration torque can be calculated by subtracting the static load torque from the motor starting torque. Fig. 8(b) displays a trajectory of the acceleration time of the ESP drive for different levels of the starting current. The static load torque is assumed to be 20% of the motor rated torque and the change in speed is assumed to be 50% of the rated speed.

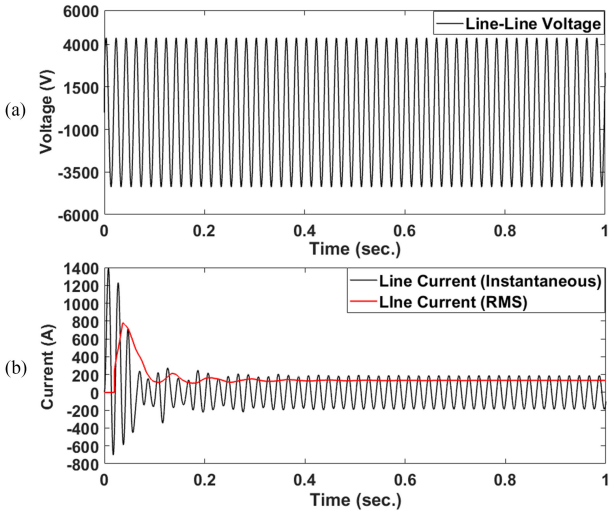

FIGURE 9. Electrical responses of the ESP during online starting: (a) voltage, and (b) line current.

IV. TORSIONAL DYNAMIC ANALYSIS OF ESP SYSTEMS

ESP systems are vulnerable to failures during start-up due to dynamic stress associated with its transient behavior. A transient model of the 750 HP ESP system is developed to investigate the impact of dynamic stress on the system's mechanical integrity. The model uses the ESP dynamics presented in Fig. 1(a) along with the soft-starter system described in Section III. The electro-mechanical systems in the ESP are connected by balancing the torque transmission through the shafts. The motor delivers the torque T_m, and the pump impellers produces counter load torques $T_{l1} - T_{l5}$. There are some additional torques due to viscous damping. The model is simulated using MATLAB/Simulink for various start-up conditions.

A. DIRECT-ON-LINE START VS. SOFT-START

Fig. 9 illustrates a direct-on-line scenario where the ESP system is started directly from the switchboard. In this case, the rated voltage is applied to the motor terminals as depicted in Fig. 9(a). The motor experiences high starting current during the acceleration period and settles down to a lower steady state value when the rotor reaches the operating speed. The starting current is almost 550% of the motor rated current as shown in Fig. 9(b). This generates significant electrical stress on the supply system. For weaker grids with a low X/R ratio, the high starting motor current may create significant voltage dips - thus prohibiting the motor to reach its rated operating speed [29]. It may also cross the limit for maximum allowable voltage drop which can force the breaker to trip.

Fig. 10 illustrates the ESP system start-up successfully using a solid-state soft-starter. In this case, a reduced pedestal voltage ($V_{\text{start}} = 0.5 * V_{\text{rated}}$) is applied to the motor terminals during starting at $t = 0$ s, the voltage is ramped up to the full rated voltage after $t = 2$ s. The voltage and current waveforms are depicted in Figs. 10(a) and 10(b), respectively. The maximum starting current is limited to 270% of the motor rated

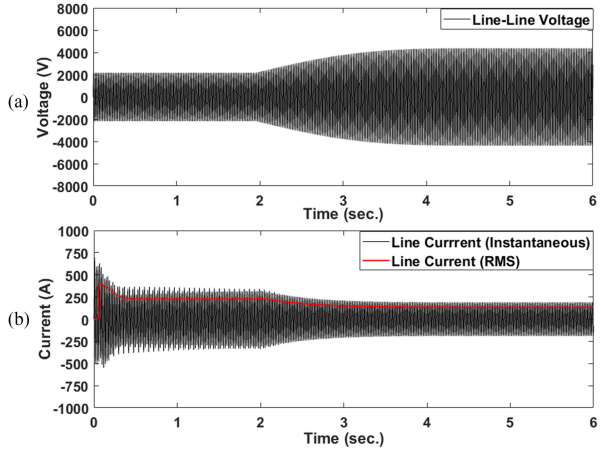

FIGURE 10. Electrical responses of the ESP during soft-starting: (a) voltage, and (b) line current.

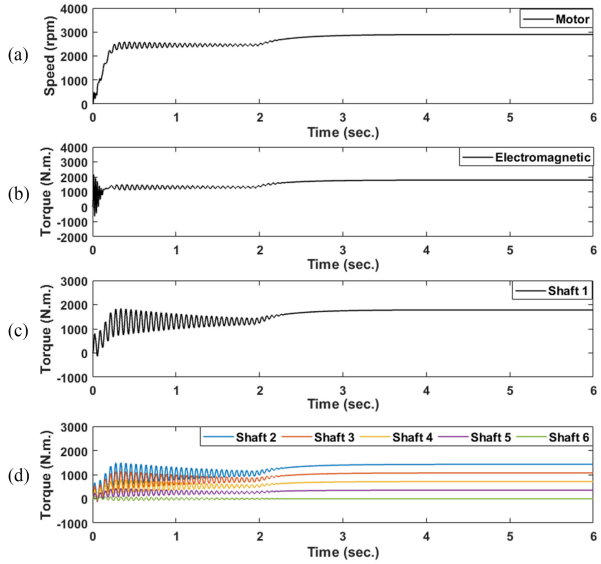

FIGURE 11. Mechanical responses of the ESP system during soft-starting: (a) motor speed, (b) motor electromagnetic torque, (c) output torque in Shaft 1, and (d) output torques in Shafts 2-6.

current whereas the average current during the acceleration is kept at 150% of the rated current by selecting the corresponding ramp up time. A lower starting current reduces the electrical stress on the supply and prevents it from significant voltage dips and unnecessary trips in the circuit breaker.

Figs. 11(a)–11(d) present the shaft dynamics of the soft-starter fed ESP drive system. The motor starting torque and the magnitude of torsional oscillations are significantly lower than its value during the direct-on-line start. This allows the rotor to start slowly from a standstill condition, avoids the severe sub-synchronous oscillations and gets stabilized to a steady state. During the ramp up, the rotor accelerates to the full load speed when the voltage is ramped up to its rated value.

Figs. 12(a) and 12(b) illustrate torsional shear stresses on Shafts 1 and 2 for direct online starting and soft-starter starting

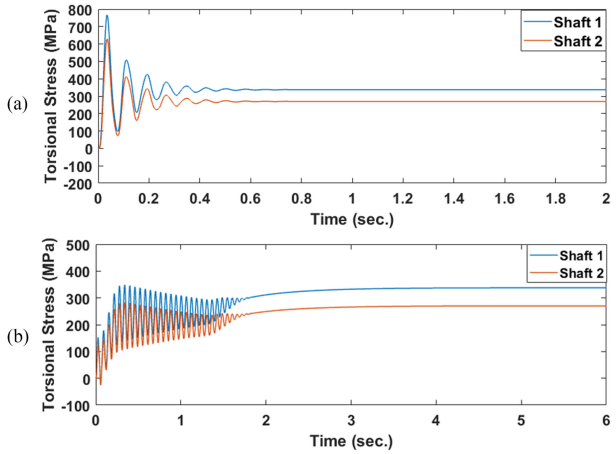

FIGURE 12. Shear stress on Shafts 1 and 2 due to torsion for: (a) direct online starting, and (b) soft-starting with reduced voltage.

with reduced voltage. The shear stress is calculated using the following expression [30],

$$\tau = \frac{Tr}{J_p} \tag{14}$$

Where, τ the shear stress on the shaft due to torsion, T is the applied torque on the shaft, r is the radius of the solid shaft and J_p is the polar moment of shaft inertia. The shear stress on Shaft 1 is higher than that on Shaft 2 because Shaft 1 transmits the highest amount of torque in the ESP system. The shafts experience higher dynamic stress during direct-on-line start but goes through less cyclic variations in stress than when fed by a soft-starter. The high level of stress associate with the direct on-line start can be severe on the mechanical assembly of an ESP system, and may lead to premature failures due to static overloading.

B. SOFT-START: FAILURE TO START

Selection of the maximum starting current for a soft-starter plays an important role on successful start-up of an ESP system. A low starting current will provide an inadequate starting torque for the rotor to reach a steady state before it can accelerate to the full load speed. A low starting current may also force the rotor to experience sub-synchronous oscillations and thus introduce high dynamic stress in the ESP shaft assembly. Fig. 13 shows a case scenario where the maximum starting current is limited to 125% of the rated current. The input voltage is around 25% of the motor rated voltage and is illustrated in Fig. 13(a). The current waveform is presented in Fig. 13(b).

The mechanical dynamics in the interconnected shaft assembly is provided in Fig. 14. Due to the low starting current, the starting torque is too low to overcome the static friction load torque. Thus, the rotor fails to accelerate and ends up operating in subsynchronous mode. This phenomenon is depicted in Fig. 14(a) (speed waveform) and Figs. 14(b)–14(c) (torque waveform). The subsynchronous

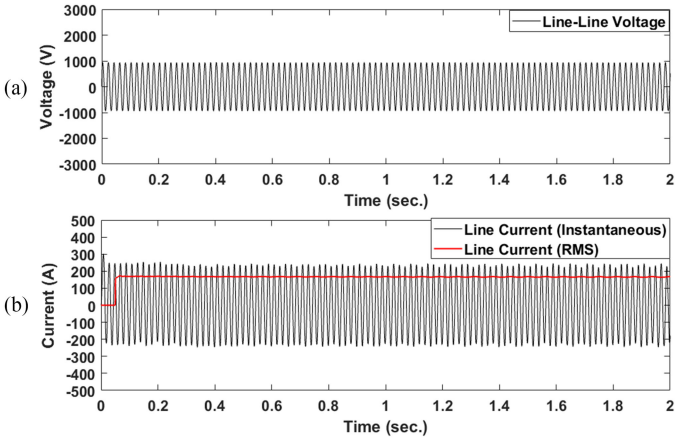

FIGURE 13. Electrical responses of the ESP during soft-starting at a low starting current: (a) voltage, and (b) line current.

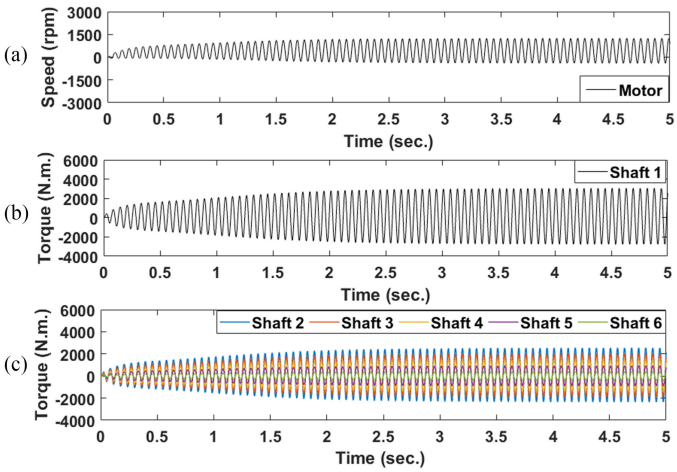

FIGURE 14. Mechanical responses of the ESP system during soft-starting at a low starting current: (a) motor speed, (b) output torque in Shaft 1, and (c) output torques in Shafts 2-6.

rotor oscillation exacerbates the torsional vibration in the shaft assembly. Shafts 1 and 2 experience the highest level of torque pulsations among the ESP shaft segments. The torque pulsations gradually decreases along the rest of the shafts as depicted in Fig. 14(c).

The shear stresses due to subsynchronous torsional oscillations on shafts 1 and 2 are presented in Fig. 15. The cyclic torsional stress becomes sustained during subsynchronous rotor oscillation and the peak amplitude of the stress gradually builds up with the severity of the oscillation. The cyclic variation in the shear stress creates fatigue in the system and can reduce the lifetime of the ESP system.

C. SOFT-START: EFFECTS OF RESONANCE

The resonance phenomenon is a critical issue in assessing shaft breakdowns in ESPs. When the frequency of the rotating shaft is close to its critical resonant frequency, the amplitude

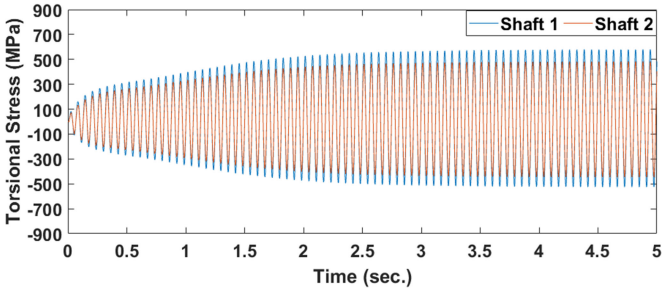

FIGURE 15. Shear stress on the shafts due to subsynchronous oscillations.

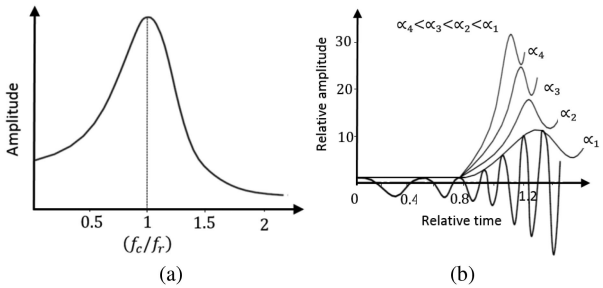

FIGURE 16. (a) Resonance effect on torsional oscillation, and (b) relative amplitude of the oscillation when passing through the resonance frequency [21].

of vibration increases, which causes serious damage such as rapid destruction, wear or fatigue. This phenomenon is depicted in Fig. 16(a). It indicates that the operation at resonance points or close to them should be avoided, and shafts should pass through one or several critical speeds quickly during the start-up in order to reach the operating speed.

Fig. 16(b) shows the phenomenon when the shaft operating speed approaches its critical speed. The amplitude of the shaft's torsional oscillations depends on its angular acceleration. The amplitude of the oscillation goes down significantly when the shaft crosses the resonant frequency with a high acceleration. Thus, in order to have an acceptable design of the shaft assembly, it is necessary to estimate the maximum amplitude of the torsional oscillations during the passing through the critical speeds. It is difficult to find the value theoretically, however, it can be estimated as follows [31]:

$$A \approx \frac{3.78}{\sqrt{2\pi\lambda}} \exp\left[-1.16\left(\frac{1}{2\pi\lambda}\right)^{0.379} D_{mp}{}^{0.7}\right] \tag{15}$$

where, A is the relative amplitude of the oscillation, and λ is the relative angular acceleration of shaft 1. The resonance frequency for Shaft 1 is calculated by assuming the motor and the pump as rotating inertial bodies. Thus, the undamped resonance frequency for Shaft 1 can be obtained by [3],

$$f_r = \frac{1}{2\pi}\sqrt{\frac{\left(\frac{1}{C_{mp}}\right) J_m J_p}{J_m + J_p}} \tag{16}$$

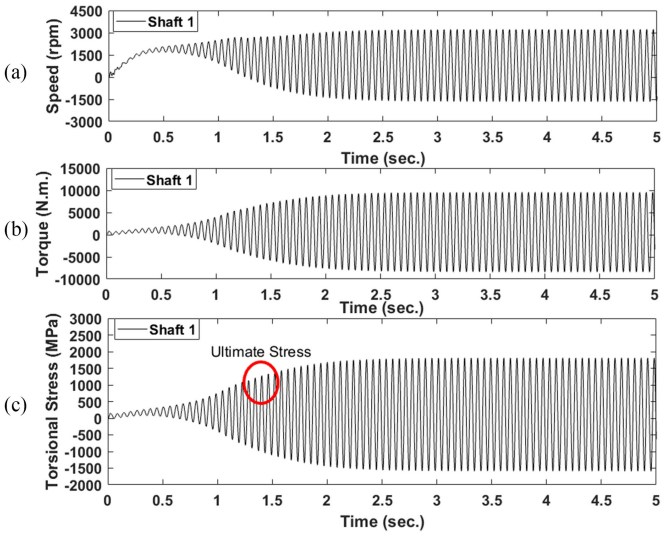

FIGURE 17. Behavior of the ESP system when experiencing resonance: (a) shaft speed, (b) torque response, and (c) induced torsional stress.

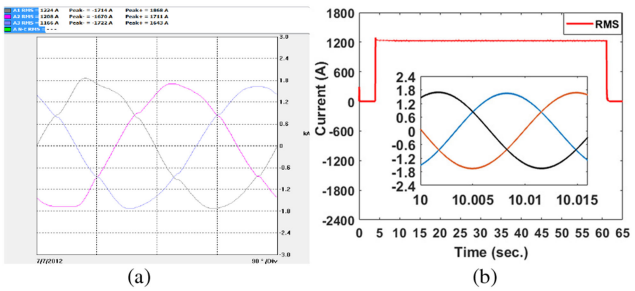

FIGURE 18. (a) Field test current, and (b) simulated current.

Where, f_r is the resonant frequency; J_m and J_p are motor and pump inertias, respectively.

Figs. 17(a)–17(c) illustrate a case scenario where the motor in the ESP drive failed to provide a sufficient acceleration for the rotor to cross the resonant frequency of Shaft 1 which is calculated as 25 Hz (1500 rpm) using (16). Thus, resonance occurs in the system and can be recognized from the growing speed oscillation in Fig. 17(a). The resonance in shaft 1 creates severe torsional oscillations in the system which induces a very high amount of stress in the system as illustrated in Figs. 17(b)–17(c). The stress level eventually crosses the ultimate stress level of the shaft as indicated by the red circle in Fig. 17(c). The shaft will be broken immediately as it happens which will cause ESP failures. Thus, care should be taken to select the proper setting for the soft-starter to avoid ESP failures due to resonance.

V. ANALYSIS OF FATIGUE IN ESP SHAFTS

Fluctuation stress resulting from insufficient starting current during soft-starting creates fatigue in an EPS's mechanical system. Fatigue is one of the root causes behind mechanical components' failure in ESPs. Under the fatigue induced operations, machine parts operating under a varying stress fail at a significantly lower stress level than its ultimate stress.

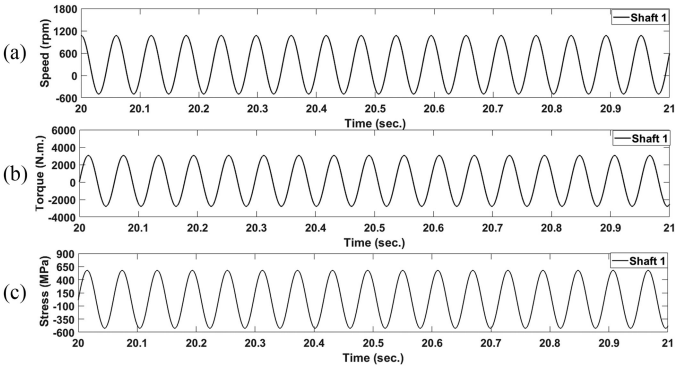

FIGURE 19. The simulated dynamic response of the ESP system: (a) speed, (b) torque, and (c) torsional stress.

Fig. 18 shows a real-world case scenario where the 750 HP ESP system in Fig. 4(a) failed to start due to a low starting current. Successive attempts were made to start the ESP system. The field test and simulated transformer primary side current waveform and its RMS values are presented in Figs. 18(a) and 18(b), respectively. The simulated performance of the ESP system using the dynamic model for the same scenario is shown in Fig. 19. Fig. 19(a) is the speed waveform. Figs. 19(b) and 19(c) are the torque and associated fluctuating torsional stresses, respectively. The midrange and amplitude of stress are calculated as follows [32]:

$$\sigma_m = \frac{\sigma_{\max} + \sigma_{\min}}{2}\ ; \quad \sigma_a = \frac{\sigma_{\max} - \sigma_{\min}}{2} \tag{17}$$

Where, $\sigma_{\max}$ and $\sigma_{\min}$ are the peak amplitudes of the positive and negative stresses. The resultant reversed stress on the shaft can be obtained by the modified Goodman failure criterion, and the equations for calculating it are expressed by [32]

$$\sigma_{rev} = \frac{\sigma_a}{1 - \frac{\sigma_m}{S_{us}}};\ S_{us} = 0.67 S_{ut} \tag{18}$$

Where, σ_{rev} is the reversed stress, and S_{ut} is the ultimate stress on the shaft. The critical number of torsional stress cycles before a shaft breakdown can be obtained by [32]:

$$N = \left(\frac{\sigma_{rev}}{a}\right)^{1/b};\ a = \frac{(f S_{us})^2}{S_e}\ ;\ b = -\frac{1}{3}\log\left(\frac{f S_{us}}{S_e}\right) \tag{19}$$

Where, N is the number of cycles-to-failures, f is the fatigue strength fraction, S_e is the endurance limit at the critical location, a and b are fatigue coefficients. The endurance limit for a shaft depends on its geometry and operating condition and can be estimated as follows [32]:

$$S'_e = 0.5\, S_{ut};\ S_e = k_a k_b k_c k_d k_e k_f S'_e \tag{20}$$

where, k_a is the surface condition factor, k_b is size modification factor, k_c is load modification factor, k_d is temperature

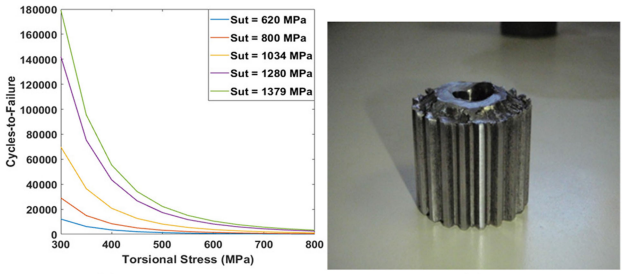

(a) (b)

FIGURE 20. **(a) Fatigue curve for different grades of steel, (b) a broken shaft.**

modification factor, k_e is reliability factor, and S'_e is rotary-beam test specimen endurance limit.

The fluctuation stress in Shaft 1 for the sustained torsional oscillation has $\sigma_{\max} = 575$ MPa and $\sigma_{\min} = -525$ MPa, and the resultant reverse stress on the shaft, $\sigma_{rev} = 567$ MPa. The total number of stress cycles in the shaft before it fails due to fatigue for different levels of reverse stress is depicted in Fig. 20(a). In this case, the system is active for 57s, and the number of cycles per second is 18. The total number of attempts has been 6, which makes the number of cycles to reach close to 6000. The ultimate strength for the shaft material is anywhere between 800 MPa and 1034 MPa. Based on Fig. 20(a), this causes the breakdown in Shaft 1 somewhere between 1700 cycles and 4600 cycles i.e., most likely after the 1st attempt. Fig. 20(b) illustrate a picture of the broken shaft during field testing of the ESP system due to this fatigue induced operation. The shaft is broken at the top of the coupling between the motor and the protector (Shaft 1), where the stress is highly concentrated.

Based on the analysis, it is evident that insufficient starting current can introduce resonance and fatigue in soft-starter fed ESP systems. It is recommended to carry out a dynamic analysis of an ESP system before choosing an appropriate current setting for the soft-starter. A safe guideline would be to apply a sufficient amount of starting current (>=250%) for few seconds that will allow the rotor to cross the critical speed before ramping up to the full load speed. In the events of start-up failures, the ESP system should be shut down immediately to avoid fatigue in the system. Multiple start-up attempts should only be taken after analyzing the root causes of the failures.

VI. CONCLUSIONS

In this paper, the broken shaft issue for reduced-voltage soft-starter fed ESP systems is investigated using a real world 750 HP ESP system through torsional dynamic stress analysis for various start-up conditions. Common ESP failure scenarios related with torsional resonance and fatigue conditions are investigated. The start-up guideline for such systems is also proposed. The proposed modeling technique can serve as a suitable tool to identify torsion related failures in an ESP system.

APPENDIX

TABLE I **Specifications of the ESP System**

Parameters	Values
The ESP rated power	750 HP
Rated voltage for Motors 1-2	1550 V@50 Hz; 1860 V@ 60 Hz
Motor rated current	147 A
Number of poles of each motor	2
Rated speed @ 50 Hz	2850 RPM
Transformer rating	630 kVA, 410V / 3031 V
Transmission line parameters	$R_{line} = 0.08\Omega$; $L_{line} = 508e-7$ H; $C_{line} = 370.4e-10$ F
Inertias	$J_m, J_p = 0.3337, 0.0265$ kg.m^2;
Dimensions for Shafts 1 and 2	Length = 2.71 m, Diameter = 30 mm
Dimensions for Shafts 3-6	Length = 2.03 m, Diameter = 30 mm
Damping in each pump stage	$D_{1-5} = 0.1333$ N. s./rad.
Load torque coefficients	a = –924.22; b = 2417.2; c= –2288.4; d =1055.4; e = –169.98

REFERENCES

[1] O. J. Romero and A. Hupp, "Subsea electrical submersible pump significance in petroleum offshore production," *ASME J. Energy Resour. Technol.*, vol. 136, no. 1, Sep. 2014, Art. no. 012902.

[2] R. Durham and T. Brinner, "Oilfield electric power distribution," *IEEE Trans. Ind. Appl.*, vol. 51, no. 4, pp. 3532–3547, Jul. 2015.

[3] O. V. Thorsen and M. Dalva, "Combined electrical and mechanical model of electric submersible pumps," *IEEE Trans. Ind. Appl.*, vol. 37, no. 2, pp. 541–547, Mar. 2001.

[4] R. L. Hyde and T. R. Brinner, "Starting characteristics of electric submersible oil well pumps," *IEEE Trans. Ind. Appl.*, vol. 22, no. 1, pp. 133–144, Jan. 1986.

[5] A. VanderMeulen, T. Natali, T. Dionise, G. Paradiso, and K. Ameele, "Exploring new and conventional starting methods of large medium-voltage induction motors on limited kVA sources," *IEEE Trans. Ind. Appl.*, vol. 55, no. 5, pp. 4474–4482, Sep. 2019.

[6] K. LeDoux, P. Visser, J. Hulin, and H. Nguyen, "Starting large synchronous motors in weak power systems," *IEEE Trans. Ind. Appl.*, vol. 51, no. 3, pp. 2676–2682, May 2015.

[7] R. Pragale and D. Shipp, "Investigation of premature ESP failures and oil field harmonic analysis," *IEEE Trans. Ind. Appl.*, vol. 53, no. 3, pp. 3175–3181, May 2017.

[8] M. Farbis, A. Hoevenaars, and J. Greenwald, "Oil field retrofit of ESPs to meet harmonic compliance," *IEEE Trans. Ind. Appl.*, vol. 52, no. 1, pp. 718–728, Jan. 2016.

[9] R. El-Mahayni, K. Al-Qahtani, and A. H. Al-Gheeth, "Large synchronous motor failure investigation: Measurements, analysis, and lessons learned," *IEEE Trans. Ind. Appl.*, vol. 52, no. 6, pp. 5318–5326, Nov. 2016.

[10] J. Dymond, "Stall time, acceleration time, frequency of starting: The myths and the facts," *IEEE Trans. Ind. Appl*, vol. 29, no. 1, pp. 42–51, Jan. 1993.

[11] K. Smith and L. Ran, "Investigation of starting dynamics of electrical submersible pumps with soft starting," in *Proc. IEE Power Electron. Variable-Speed Drives Conf.*, London, U.K., Oct. 1994, pp. 586–590.

[12] J. Larabee, B. Pellegrino and B. Flick, "Induction motor starting methods and issues," in *Proc. IEEE PCIC Elect. Safety Workshop*, Denver, CO, USA, Feb. 2005, pp. 217–222.

[13] P. Zhang, J. Dai, T. Habetler., and B. Lu, "Impaired-cooling-condition detection using dc-signal injection for soft-starter-connected induction motors," *IEEE Trans. Ind. Elect.*, vol. 56, no. 11, pp. 4642–4650, Nov. 2009.

[14] P. Zhang, B. Lu, and T. Habetler., "A remote and sensorless stator winding resistance estimation method for thermal protection of soft-starter-connected induction machines," *IEEE Trans. Ind. Elect.*, vol. 55, no. 10, pp. 3611–3618, Oct. 2008.

[15] J. Liu, T. Nondahl, P. Schmidt, S. Royak, and T. Rowan, "Generalized stability control for open-loop operation of motor drives," *IEEE Trans. Ind. Appl.*, vol. 53, no. 3, pp. 2517–2525, May 2017.

[16] G. Cunha, A. Rossa, J. Alves, and E. Cardoso, "Control of permanent magnet synchronous machines for subsea applications," *IEEE Trans. Ind. Appl.*, vol. 54, no. 2, pp. 1899–1905, Mar. 2018.
[17] C. Mayer, "Torsional vibration problems and analyses of cement industry drives," *IEEE Trans. Ind. Appl.*, vol. 17, no. 1, pp. 81–89, Jan. 1981.
[18] A. Shaltout, "Analysis of torsional torques in starting of large squirrel cage induction motors," *IEEE Trans. Energy Convers.*, vol. 9, no. 1, pp. 135–142, Mar. 1994.
[19] L. Ran, R. Yacamini, and K. Smith, "Torsional vibrations in electrical induction motor drives start-up," *ASME Trans.*, vol. 118, pp. 242–251, Apr. 1996.
[20] H. Guo, Z. Lv, Z. Wu, and Bo Wei, "Multi-physics design of a novel turbine permanent magnet generator used for downhole high-pressure high-temperature environment," *IET Elect. Power Appl.*, vol. 7, no. 3, pp. 214–222, Mar. 2013.
[21] A. Bonnett, "Root cause AC motor failure analysis with a focus on shaft failures," *IEEE Trans. Ind. Appl.*, vol. 36, no. 5, pp. 1435–1448, Sep. 2000.
[22] J. Bredthauer and N. Struck, "Starting of large medium voltage motors: Design, protection, and safety aspects," *IEEE Trans. Ind. Appl.*, vol. 31, no. 5, pp. 1167–1176, Sep. 1995.
[23] N. Derbel, M. Kamoun, and M. Poloujadoff, "On the order reduction of induction machine during start-up," *IEEE Trans. Energy Convers.*, vol. 10, no. 4, pp. 655–660, Dec. 1995.
[24] J. Shadley, B. Wilson, and M. Dorney, "Unstable self-excitation of torsional vibration in ac induction motor driven rotational systems," *ASME Trans.*, vol. 114, pp. 226–231, Apr. 1992.
[25] G. R. Slemon, *Electric Machines and Drives*. New York, NY, USA: Addison-Wesley, 1992.
[26] M. H. Rashid, *Power Electronics, Devices, Circuits and Applications*. London, U.K.: Pearson Education, 2014.
[27] A. Boglietti, A. Cavagnino, and M. Lazzari, "Computational algorithms for induction-motor equivalent circuit parameter determination—part I: Resistances and leakage reactances," *IEEE Trans. Ind. Electron.*, vol. 58, no. 9, pp. 3723–3733, Sep. 2011.
[28] A. Boglietti, A. Cavagnino, and M. Lazzari, "Computational algorithms for induction motor equivalent circuit parameter determination—part II: Skin effect and magnetizing characteristics," *IEEE Trans. Ind. Electron.*, vol. 58, no. 9, pp. 3734–3740, Sep. 2011.
[29] S. Hasan, N. Gurung, K. Muttaqi, and S. Kamalasadan, "Electromagnetic field-based control of distributed generator units to mitigate motor starting voltage dips in power grids," *IEEE Trans. Appl. Supercond.*, vol. 29, no. 2, Mar. 2019, Art. no. 0602604.
[30] H. Dresig H, and F. Holzweißig, *Dynamics of Machinery: Theory and Applications*. Berlin, Germany: Springer, 2010.
[31] Y. Ishida and T. Yamamoto, *Linear and Nonlinear Rotordynamics*. Hoboken, NJ, USA: Wiley, 2012.
[32] R. Budynas and J. Nisbett, *Shigley's Mechanical Engineering Design*. New York, NY, USA: McGraw-Hill, 2011.

SHEIKH F. RABBI (S'12–M'17) was born in Bogra, Bangladesh. He received the B.Sc. degree (first class honors) in computer science and engineering from the Bangladesh University of Engineering and Technology (BUET), Dhaka, Bangladesh, in 2009 and the M.Eng. and Ph.D degrees in electrical engineering from the Memorial University of Newfoundland (MUN), St. John's, NL, Canada in 2012 and 2017, respectively.

After completing the Ph.D. degree, he founded DuXion where he is currently leading the development of electric propulsion systems for aircraft. From February 2019 to February 2020, he is a Postdoctoral Fellow with the Department of Electrical and Computer Engineering, MUN. His research interest includes permanent magnet machines, electric propulsion, submersible drives, control systems, power electronics, and renewable energy.

Dr. Rabbi has been the recipient of numerous awards and honors, including Ph.D. Distinction Award (MUN), fellow of the School of Graduate Studies (MUN), the University Merit Scholarship (BUET), Dean's List (BUET), IEEE CCECE 2015 Best Paper Finalist Award, IEEE ECCE 2015 Student Travel Grant Award, the IEEE NECEC Wally Read Best Young Professional Paper Award in 2014 and the IEEE NECEC Wally Read GOLD Best Conference Paper Awards in 2012 and 2013, respectively.

JALAL TAHERI KAHNAMOUEI was born in Tabriz, Iran. He received the B.Sc. degree in mechanical engineering from IAU-Tabriz University, Tabriz, Iran in 2006, and the M.Sc. degree in mechanical engineering from IAU- Science and Research Branch of Tehran University, Tehran, Iran in 2009. Since 2015, he has been working toward the Ph.D. degree in mechanical engineering with the Memorial University of Newfoundland, St. John's, NL, Canada. His research interests include dynamics, vibration, renewable energy, wind turbine and rotary machine dynamics.

From 2009 to 2015, he worked as a Mechanical Engineer in automation and iron-making industries. Also, he served as an Adjunct Lecturer at IAU University and the University of Applied Science and Technology.

XIAODONG LIANG (M'06–SM'09) was born in Lingyuan, China. She received the B.Eng. and M.Eng. degrees from Shenyang Polytechnic University, Shenyang, China in 1992 and 1995, respectively, the M.Sc. degree from the University of Saskatchewan, Saskatoon, SK, Canada in 2004, and the Ph.D. degree from the University of Alberta, Edmonton, AB, Canada, in 2013, all in electrical engineering. Her research interests include power systems, renewable energy, and electric machines.

From 1995 to 1999, she was a Lecturer with Northeastern University, Shenyang, China. In October 2001, she joined Schlumberger in Edmonton, Canada, and in 2009 was promoted to be a Principal Power Systems Engineer with this world's leading oil field service company. After serving Schlumberger for almost 12 years, from 2013 to 2019, she was with Washington State University in Vancouver, United States and the Memorial University of Newfoundland in St. John's, Canada as an Assistant and later Associate Professor. In July 2019, she joined the University of Saskatchewan in Saskatoon, Canada, where she is currently an Associate Professor.

Dr. Liang is a registered Professional Engineer in the province of Saskatchewan, Canada.

JIANMING YANG was born in China in 1964. He received the Ph.D. degree in mechanical engineering from Tianjin University, Tianjin, China, in 2001. From 2001 to 2003, he was a Postdoctoral Researcher with Shanghai Jiaotong University, China. From 2003 to 2006, he worked with the Universuty of Shanghai for Science and Technology first as an Associate Professor, and then a Full Professor. Since 2010, he has been with the Department of Mechanical Engineering, Memorial University of Newfoundland, Canada, where he is currently an Associate Professor. His research interests include vibration, dynamics, fatigue of mechanical systems and components.

Dr. Yang is a registered Professional Engineer in the province of Newfoundland and Labrador, Canada.